Cell Research (2008) 18:479-490.

www.nature.com/cr

ORIGINAL ARTICLE

Migratory properties of cultured olfactory ensheathing cells by single-cell migration assay

Zhi-hui Huang[1,2], Ying Wang[1], Li Cao[2], Zhi-da Su[2], Yan-ling Zhu[2], Yi-zhang Chen[1,2], Xiao-bing Yuan[3], Cheng He[1,2]

[1]Department of Neurobiology, Institute of Neuroscience, Zhejiang University School of Medicine, Hangzhou, Zhejiang 310058, China; [2]Department of Neurobiology, Second Military Medical University, Shanghai 200433, China; [3]Institute of Neuroscience, Shanghai Institutes for Biological Sciences, Chinese Academy of Sciences, Shanghai 200031, China

Olfactory ensheathing cells (OECs) are a unique type of glial cells that have axonal growth-promoting properties. OEC transplantation has emerged as a promising experimental therapy of axonal injuries and demyelinating diseases. However, some fundamental cellular properties of OECs remain unclear. In this study, we found that the distinct OEC subpopulations exhibited different migratory properties based on time-lapse imaging of single isolated cells, possibly due to their different cytoskeletal organizations. Moreover, OEC subpopulations displayed different attractive migratory responses to a gradient of lysophosphatidic acid (LPA) in single-cell migration assays. Finally, we found that OEC subpopulations transformed into each other spontaneously. Together, these results demonstrate, for the first time to our knowledge, that distinct OEC subpopulations display different migratory properties *in vitro* and provide new evidence to support the notion of OECs as a single cell type with malleable functional phenotypes.

Keywords: olfactory ensheathing cells, motility, morphology, LPA, single-cell migration

Cell Research (2008) **18**:479-490. doi: 10.1038/cr.2008.38; published online18 March 2008

Introduction

The adult mammalian olfactory system is unusual in that olfactory neurons are regularly renewed throughout life [1]. This remarkable regenerative property of the olfactory system is thought to be in part due to a special type of glia cells [2, 3], the olfactory ensheathing cells (OECs), which support and guide the growth of olfactory axons and ensheath the bundles of olfactory nerves that extend from the olfactory epithelium to the olfactory bulb [4]. Owing to these unique roles, OEC transplantation has emerged as a promising experimental therapy for axonal injuries and demyelinating disease [5]. Experimental studies have shown that OECs transplanted near nerve injury sites can not only promote the re-growth of injured axons [6-8], but also form myelin sheaths around demyelinated axons, leading to the restoration of axonal functions [9-15]. Moreover, transplantation of autologous OECs into the injured spinal cord in human is feasible and is safe up to 1 year after implantation [16].

Although OECs have been successfully used in many transplantation experiments with encouraging outcomes, some fundamental cellular properties of OECs remain unclear, such as their motility under different physiological conditions. The migratory ability of OECs is important for the development of the olfactory system and neural regeneration [11, 17-19]. During embryonic development, OECs are derived from olfactory placode, migrate out of the olfactory epithelium along the olfactory axons from the lamina propria, go through the cribriform plate into the cranial cavity and finally form the glia limitations surrounding the olfactory bulb [17]. The elongation of olfactory axons through the lamina propria may be largely attributed to the behavior of the migrating OECs that accompany the nerve fibers [20]. Several studies have reported that distinct OEC subpopulations exist in the olfactory system, based on their morphology and antigenic profiles [4, 21, 22]. For example, OECs from the lamina propria express unique developmentally important proteins such as NG2, which is not expressed in OECs from the olfactory bulb [22]. However, whether these distinct OEC subpopulations

Correspondence : Cheng He
Tel: +86 21 65515200; Fax: +86 21 65492132
E-mail: chenghe@online.sh.cn
Received 3 August 2007; revised 22 October 2007; accepted 31 October 2007; publised online 18 March 2008

display different migratory properties during embryonic development is not clear.

After transplantation, OECs can migrate a long distance from the area of surgical placement to the lesion site and can associate with extending axons [8, 9, 11, 23, 24]. The migratory properties of OECs are thought to account for their repair qualities. Cultured OECs have been described as two subpopulations [25-27]. One subpopulation is known as the Schwann cell-like OECs, which have a long fusiform bipolar morphology; the other is known as the astrocyte-like OECs, which have a flat sheet-like morphology. Interestingly, several studies have shown that Schwann cell-like OECs are more effective in promoting axonal regeneration than astrocyte-like OECs *in vitro* and *in vivo* [11, 28-30]. Transplanted OECs from the lamina propria and olfactory bulb, which display differential integration and migration, promote differential axonal sprouting in the lesioned spinal cord [31]. However, little is known about the migratory properties of these OEC subpopulations.

In this study, we examined the migratory properties of these distinct OEC subpopulations *in vitro*. Based on time-lapse imaging of the migratory behavior of single isolated OECs, we found that OEC subpopulations exhibit remarkable difference in their motility.

Results

OEC subpopulations exhibit different migratory properties

Consistent with previous reports [25], OECs displayed mainly two kinds of morphology in the primary culture system. One was the Schwann cell-like morphology, with two processes and a long fusiform bipolar form (Figure 1A a); the other was the astrocyte-like morphology, with short randomly orientated processes and flat sheet-like shape (Figure 1A b, c). In our studies, however, the latter could be further divided into two subtypes according to the location of the nucleus. As shown in Figure 1A b, astrocyte-like type 1 OECs were defined as those exhibiting a fan-like shape, with a nucleus lying at the edge of cytoplasm and a large lamellipodium extending from the opposite side to the nucleus. Astrocyte-like type 2 OECs were defined as those having a round shape and a nucleus lying at the center of cytoplasm (Figure 1A c). The proportion of each morphological type in the cultures changed with the length of culture time. The proportion of Schwann cell-like OECs significantly decreased from 48.5% at 12 h to 33.3% at 36 h, and astrocyte-like type 2 cells significantly increased from 24.3% at 12 h to 41% at 36 h (Supplementary information, Figure S1); however, the proportion of astrocyte-like type 1 cells changed little.

To further confirm whether cells with different shapes were genuine OECs in our culture system, we chose the OEC markers S-100, $p75^{NTR}$ and GFAP to identify them [15, 22, 34]. We performed double-label immunostaining for these subpopulations. Only cells that were immunopositive for two markers were counted as OECs (see Materials and Methods). As shown in Figure 1B, C, Schwann cell-like OECs were immunopositive for $p75^{NTR}$ and GFAP (97.3%), $p75^{NTR}$ and S-100 (96.3%), and S-100 and GFAP (96.5%). Astrocyte-like type 1 OECs were also very pure because they were immunopositive for $p75^{NTR}$ and GFAP (94.8%), $p75^{NTR}$ and S-100 (95%), and S-100 and GFAP (95.3%). Astrocyte-like type 2 OECs were immunopositive for $p75^{NTR}$ and GFAP (91.8%), $p75^{NTR}$ and S-100 (91.5%), and S-100 and GFAP (90.5%). The high purity of each OEC subpopulation reinforced our classification of OECs and experiments as follows.

To examine the migratory properties of these distinct OEC subpopulations, we developed a single-cell migration assay (see Materials and Methods). Under the microscope, we selected cells with typical OEC morphology that had no contact with any other cells. Based on time-lapse imaging of the migratory behavior of single isolated OECs, we found that there were three major modes of OEC migration, which were adopted by the three OEC subpopulations (Figure 2 and Supplementary information, Movies 1-3).

The first mode of migration was adopted by the Schwann cell-like OECs (Figure 2A), which had a bipolar fusiform shape. They sent out two processes during migration. One of the processes that had larger lamellipodia and/or higher dynamic filopodia and extended in the direction of cell migration was considered the 'leading process'; the other process in the opposite direction that had smaller lamellipodia and/or less dynamic filopodia was considered the 'trailing process'. As the leading process moved ahead, the nucleus of the OEC moved forwards simultaneously. Meanwhile, the trailing process underwent gradual retraction, with transient extension at its tip in some cases.

The second mode of migration was adopted by most astrocyte-like type 1 OECs (Figure 2B a). These cells did not have an obvious leading process and trailing process, but had one large lamellipodium extending forwards, with the soma following at the back. The entire cell moved as a unit, maintaining its fan-like morphology during migration.

In the third mode (Figure 2B b), the OECs were mobilized by extensions and retractions of the lamellipodia and filopodia. The cell had a disk-like shape with its nucleus at the center of the cell. The lamellipodia and filopodia adhered to the substrate with the tips extending and retracting constantly. The entire cell also moved as a unit at a very slow rate. This migration mode was mainly adopted by astrocyte-like type 2 OECs.

To quantify the motility of each OEC subpopulation,

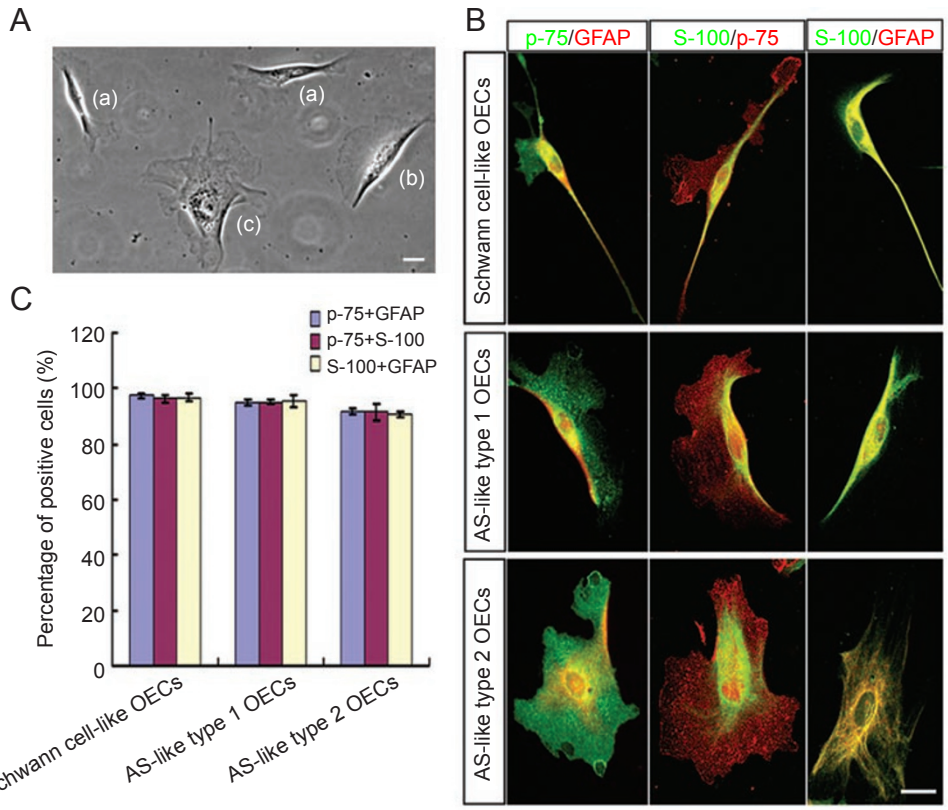

Figure 1 Characterization of OEC subpopulations. **(A)** OEC phases in primary cultures. OECs were classified as Schwann cell-like OECs with a long fusiform bipolar morphology (a) and astrocyte-like OECs with a flat sheet-like morphology (b,c). The latter was divided into astrocyte-like type 1 OECs (b) and astrocyte-like type 2 OECs (c) according to the location of the nucleus. **(B)** Double-labeled immunostaining of OEC subpopulations by p-75, GFAP and S-100. **(C)** A histogram showing the purity of different OEC subpopulations by calculating the ratio of immunopositive cells (p-75, S-100, GFAP) in total counted cells. Cells were counted in at least 20 randomly selected fields from one coverslip and 100 cells for each subpopulation per coverslip (n = 4) were counted. AS, astrocyte, scale bars = 20 μm.

we measured the migration rate on the laminin substrate of 26 cells in each OEC subpopulation, and plotted the data on a cumulative distribution graph as shown in Figure 2C. Statistical analysis of the distribution indicated a significant difference in the motility among the different OEC subpopulations. Schwann cell-like OECs were more motile than astrocyte-like OECs. Interestingly, astrocyte-like type 1 OECs had higher motility than astrocyte-like type 2 OECs. This tendency was also reflected in the average migration rates of the OEC subpopulations (Figure 2D).

To further study the motility differences between the OEC subpopulations, we next examined OEC migration on other culture substrates, including Matrigel, collagen gel, and poly-L-lysine (PLL). As shown in Figure 3, quantitative analysis of the motilities of the OEC subpopulations on these three substrates showed similar results to those found on laminin, with Schwann cell-like OECs being more motile than astrocyte-like OECs and astrocyte-like type 1 OECs having higher motility than astrocyte-like type 2 OECs.

OEC subpopulations have different cytoskeletal organizations

Since the reorganization of the cytoskeleton is essential for cell motility [38], we next examined whether different motilities of OEC subpopulations could be attributed to the different expression patterns of F-actin and microtubule cytoskeleton. To visualize F-actin and the microtubules, OEC was fixed and simultaneously labeled for F-actin using rhodamine-conjugated phalloidin and microtubules with specific antibody against acetylated α-tubulin, the marker for stable microtubules. As shown in Figure 4A, in the Schwann cell-like OECs, actin filaments were predominant in the peripheral domain of lamellipodia, whereas bundles of microtubules were localized to the central domain, parallel to the F-actin bundles. A few free microtubules penetrated into the peripheral domain. However, in astrocyte-like type 1 OECs, bundles of microtubules extended

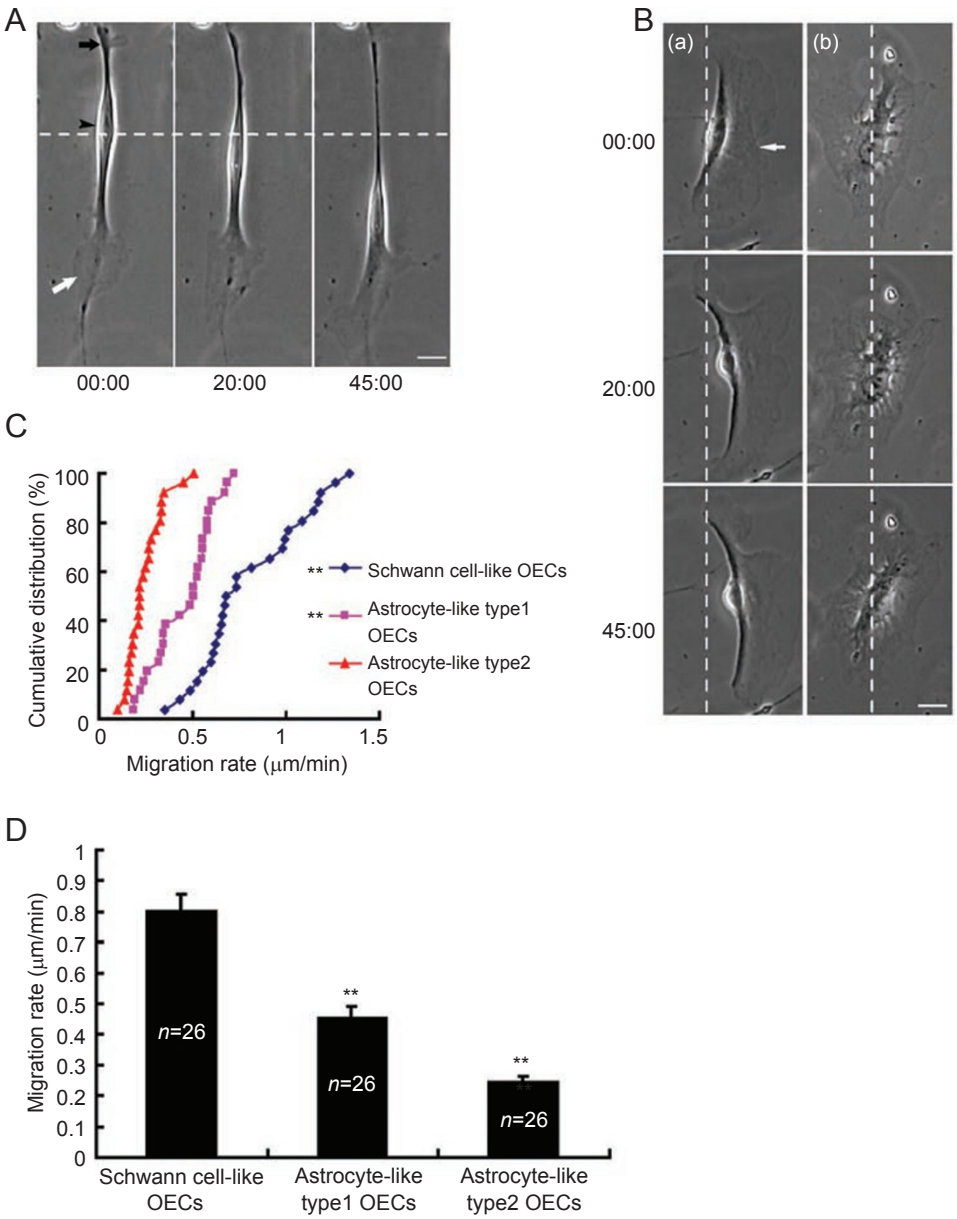

Figure 2 OEC subpopulations display different migratory properties on a laminin substrate. **(A)** In the first migration mode, OECs have a bipolar fusiform shape. When moving, the leading process (white arrow) and the OEC nucleus (black arrowhead) moved forwards simultaneously. Meanwhile, the trailing process (black arrow) underwent gradual retraction. **(B)** (a) In the second mode, OECs have a fan-like shape, with one large lamellipodium (white arrow) extending to the front and the soma following at the back. Entire OECs move as a unit. (b) In the third mode, OECs with a disk-like shape were mobilized by extending or retracting their lamellipodia and filopodia. **(C)** Cumulative distribution of the migration rates of OEC subpopulations. Each point represents the result from one OEC (n = 26). The distribution of Schwann cell-like OECs was significantly different from that of astrocyte-like OECs (**P < 0.01, Kolmogorov–Smirnov test), and the distribution of astrocyte-like type 1 OECs also was significantly different from that of astrocyte-like type 2 OECs (**P < 0.01, Kolmogorov–Smirnov test). **(D)** Histogram showing the average migration rate of the different OEC subpopulations. Data are presented as the mean ± SEM and evaluated using an ANOVA with pair-wise comparisons. **P < 0.01. Scale bars = 20 μm, time = min.

into the peripheral domain of lamellipodia (Figure 4B). In astrocyte-like type 2 OECs, microtubules radiated from the central region of the cell towards the cell periphery, and thick bundles of F-actin were aligned in lamellipodia (Figure 4C), a phenotype that was not observed in the other two types of OECs. This kind of alignment of thick F-actin

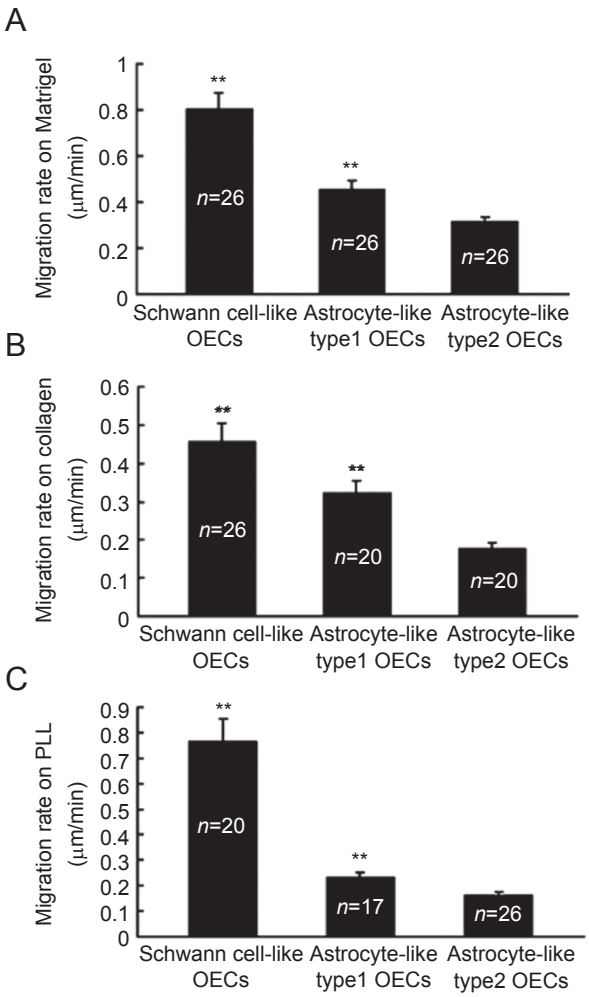

Figure 3 OEC subpopulations display different motilities on three other substrates. Histograms show the average migration rates of the distinct OEC subpopulations on Matrigel **(A)**, collagen **(B)** and PLL **(C)**. Data are presented as the mean ± SEM and evaluated using an ANOVA with pair-wise comparisons. $^{**}P < 0.01$.

bundles may stabilize the morphology of astrocyte-like type 2 cells and reduce their motility. Altogether, these results clearly demonstrate that the different OEC subpopulations exhibit a distinct distribution of cellular cytoskeleton, which may account for the difference in their motility.

OEC subpopulations have different responses upon lysophosphatidic acid (LPA) stimulation

The above results show that the OEC subpopulations display different motility during their free migration on the same substrate. We next examined whether the distinct OEC subpopulations have different responses to the same migratory factor. Here, we developed a novel directional migration assay, which was adapted from an axon growth cone turning assay [35] and a single neuron migration assay [36]. To perform this assay, a microscopic gradient of migratory cue was produced by repetitive puffing of the solutions containing the candidate cues through a micropipette placed at a distance of 100 μm in front of the soma of migrating OECs to mimic the gradient of migratory cues *in vivo*. Under this standard condition, the concentration of factor at a distance of 100 μm from the pipette tip was about 10^{-3} fold lower than in the pipette. Here, we tested the migratory cue LPA, which has been reported to promote the migration of OECs by using the trans-well migration assay [39].

First, we examined whether LPA could promote Schwann-like OEC migration in this assay. One migrating Schwann cell-like OEC was monitored for a control period to measure the spontaneous migratory rate. A microscopic gradient of LPA was then applied in front of the migrating

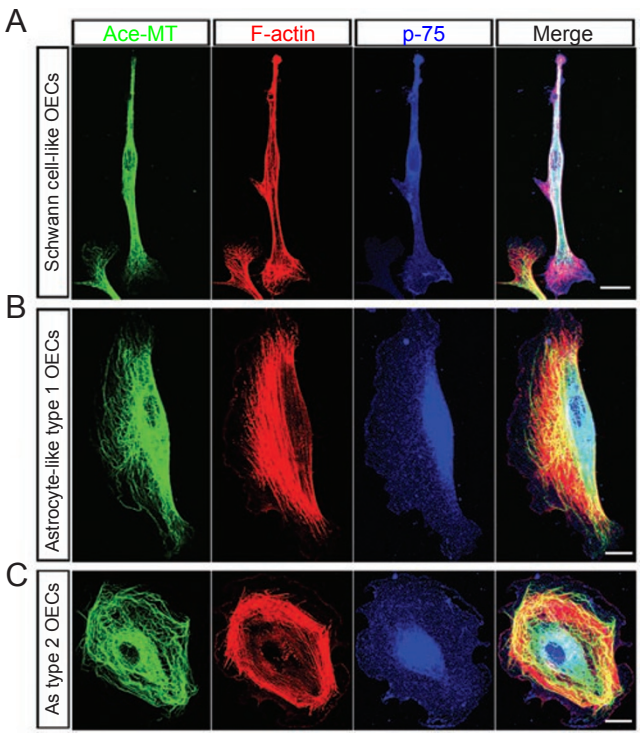

Figure 4 Distribution of cellular cytoskeleton in the OECs subpopulations. Triple immunostaining for OECs, ace-MTs (green, specific acetylated tubulin antibody), F-actin (red) and p-75 (blue, OEC marker). **(A)** In Schwann cell-like OECs, actin filaments were predominant in the peripheral domain of the lamellipodium, whereas bundles of microtubules were localized at the central domain. A few bundles of microtubules extended into the peripheral lamellipodium. **(B)** In astrocyte-like type 1 OECs, bundles of microtubules penetrated into the peripheral domain. **(C)** In astrocyte-like type 2 OECs, microtubules radiated from the central region of the cell towards the periphery, and thick bundles of F-actin aligned in the lamellipodium. As, astrocyte-like, scale bars = 20 μm.

OEC. As illustrated in Figure 5B, within minutes after onset of the LPA gradient, the cell appeared to have enhanced motility compared with the control period. The leading process became longer and the lamellipodia became larger with increased dynamics. Finally, the cell was attracted to the tip of the micropipette. During this process, the nucleus moved ahead, while the trailing process retracted rapidly. By contrast, when the micropipette was loaded with PBS, the OEC migration was unaffected compared with the control period (Figure 5A). To compare the effect of LPA on the migration of OEC subpopulations, we measured the migration rates of the leading process, the soma and the trailing process after onset of the LPA gradient, normalized these values to those obtained during the control period (which we refer to as the migration rate ratio), and plotted the data on a cumulative distribution graph as shown in Figure 5C. A ratio >1 implies that migration is faster after treatment than before, which means that this treatment can promote OEC migration; conversely, A ratio <1 implies that migration is slower after treatment than before, which means that this treatment can inhibit OEC migration. We found most migration ratios in the presence of the LPA gradient were >1 (Figure 5C). Statistical analysis of the distribution (using the Kolmogorov–Smirnov test) indicated a significant right shift in the distribution graph after onset of the LPA gradient compared with the control migratory cells, with the average migration ratio under a LPA gradient significantly increased (Figure 5D). Thus, LPA promoted the migration of Schwann cell-like OECs.

We also found that LPA could promote the migration of astrocyte-like type 1 OECs. As shown in Figure 6A, the migration of astrocyte-like type 1 OECs was accelerated by a frontal gradient of LPA. Statistical analysis of the cumulative distribution revealed significant elevation in the migratory rate of OECs cells after onset of the LPA gradient compared with the control group (Figure 6C). Also,

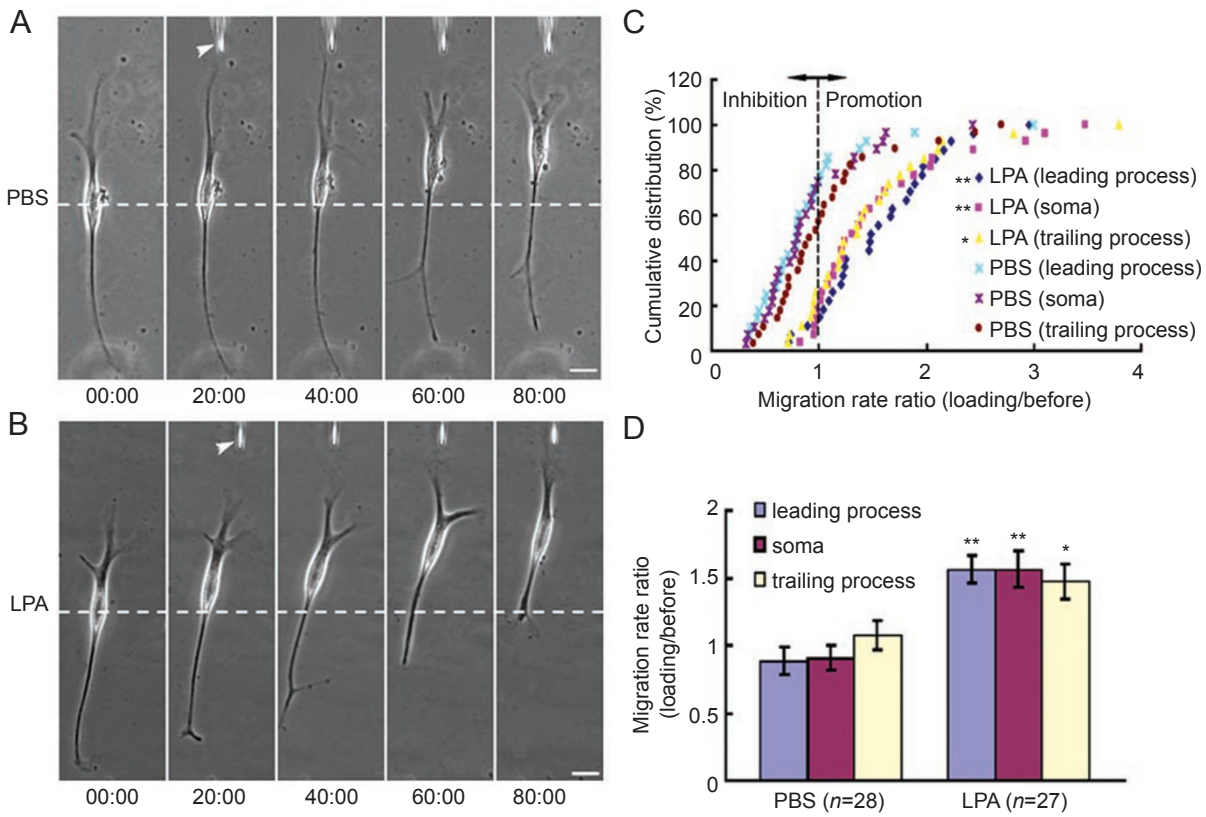

Figure 5 LPA promotes the migration of Schwann cell-like OECs in a single-cell migration assay. OEC stimulation by a gradient of LPA **(B)**, with PBS as a control **(A)**, using a micropipette (white arrowhead). **(C)** Cumulative distribution of the migration rate ratio of the leading process, the soma, and the trailing process of Schwann cell-like OECs. A migration ratio of >1 represents promotion, a ratio of < 1 represents inhibition. (We describe the migration ratio in Supplementary Figure 3 in more detail.) Each point represents the result from one OEC. The distribution of the LPA group was significantly different from the PBS group (**P < 0.01, *P < 0.05, Kolmogorov–Smirnov test). **(D)** Histogram showing the average migration rate ratio of the LPA group and PBS group. Data are presented as the mean ± SEM, and evaluated using Student's t test. **P < 0.01, *P < 0.05, difference from the PBS group. LPA, 500 μM in the pipette, scale bars = 20 μm, time in min.

the average migration ratio was significantly increased by the LPA gradient (Figure 6D). However, for astrocyte-like type 2 OECs, there was no significant difference in migration ratio between the LPA-treated group and the control group (Figure 6B-6D), suggesting that LPA did not affect their migration.

Taken together, these results indicate that the OEC subpopulations have different responses to LPA stimulation. As an attractive factor, LPA may promote the migration of Schwann cell-like OECs and astrocyte-like type 1 OECs, but not astrocyte-like type 2 OECs.

OEC subpopulations can spontaneously transform into each other

In the course of time-lapse imaging, we found that these distinct OEC subpopulations could spontaneously transform into each other, independent of any environmental stimuli. As shown in Figure 7A, one OEC displayed a typical morphology of Schwann cell-like OECs at the start of the time-lapse recording, but then rapidly transformed into an astrocyte-like type 1 OEC. During this transformation process, the leading process of this cell moved forward accompanied by enlarged lamellipodia, while there was a gradual retraction of the trailing process. After about half an hour, the leading process continued to move ahead, while the trailing process largely retracted. Finally, the trailing process completely retracted and disappeared, and the leading process became a large lamellipodium. The entire cell became a typical astrocyte-like type 1 OEC. Quantitative analysis revealed that 22% of 51 Schwann cell-like OECs transformed into astrocyte-like type 1 OECs in 1 h (Figure 7E).

We also observed that single astrocyte-like type 1 OECs rapidly transformed into Schwann cell-like OECs. As shown in Figure 7B, the lamellipodia of this astrocyte-like type 1 OECs cell gradually became smaller and longer, then the lamellipodia in the middle of the soma disappeared and the lamellipodia at the two ends of the cell were enlarged and elongated, and slowly grew into two processes. Finally, this cell became bipolar, a typical morphology of Schwann cell-like OECs. We found that 22% of 55 astrocyte-like type 1 OECs transformed into Schwann cell-like OECs in 1 h (Figure 7E).

Interestingly, two subtypes of astrocyte-like OECs also could transform into each other. As shown in Figure 7C, this astrocyte-like type 1 OEC slowly grew lamellipodia

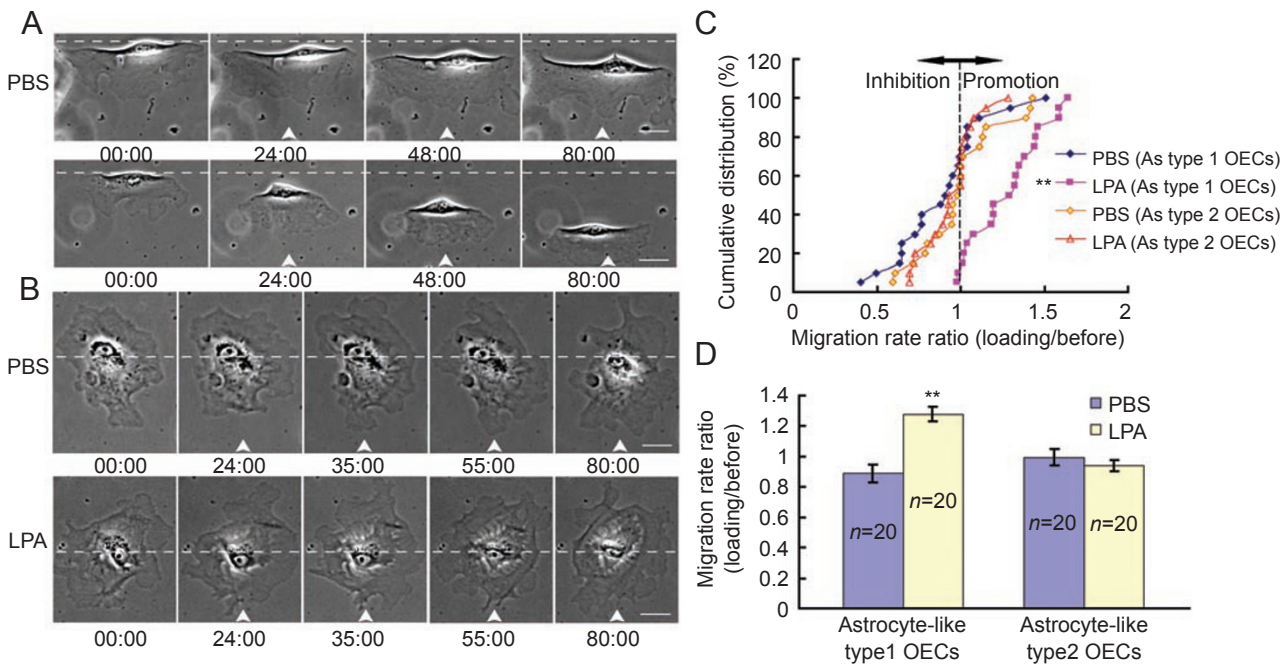

Figure 6 LPA promotes the migration of astrocyte-like type 1 OECs but not astrocyte-like type 2 OECs in a single-cell migration assay. LPA stimulates astrocyte-like type 1 **(A)** and astrocyte-like type 2 OECs **(B)**; PBS was used as the control. The white arrowhead represents the micropipette. **(C)** Cumulative distribution of the migration rate ratio of astrocyte-like OECs. The distribution of the LPA group in astrocytes like type 1 OECs was significantly different from that of the PBS group (***P* < 0.01, Kolmogorov–Smirnov test). **(D)** Histogram showing the average migration rate ratio of the LPA group and PBS group. Data are presented as the mean ± SEM and were evaluated using Student's *t* test. ***P* < 0.01 difference from the PBS group. LPA, 500 μM in the pipette, scale bars = 20 μm, time in min.

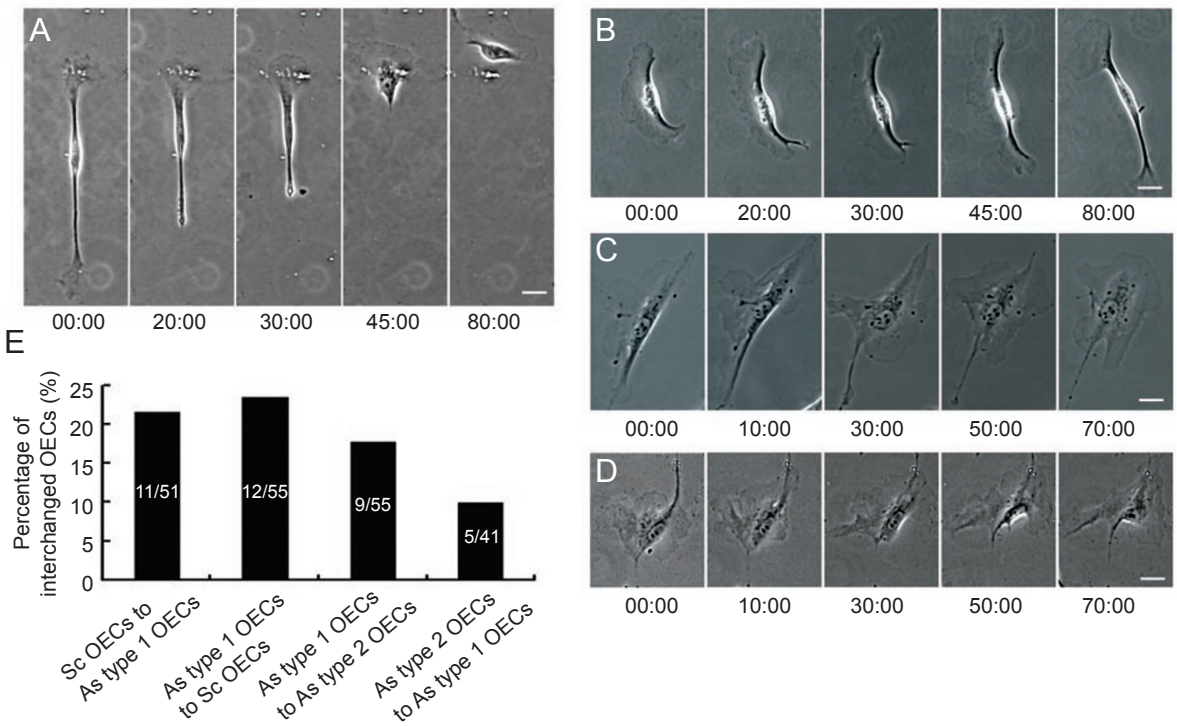

Figure 7 OEC subpopulations can transform into each other spontaneously. The example cells are shown in a series of time-lapse images **(A-D)**. **(A)** A Schwann cell-like OEC gradually transformed into an astrocyte-like type 1 OEC. **(B)** The OEC started with a typical astrocyte-like type 1 OEC and transformed into a bipolar fusiform Schwann cell-like OEC after 1 h. **(C)** An astrocyte-like type 1 OEC rapidly transformed into an astrocyte-like type 2 OEC. **(D)** An astrocyte-like type 2 OEC transformed into an astrocyte-like type 1 OEC, and finally it changed back to the type 2 rapidly. **(E)** Histogram showing the percentages of transformed OECs in total observed cells. Sc, Schwann cell-like; As, astrocyte-like. Scale bars = 20 μm, time in min.

near the side of the nucleus, and the nucleus located to the center of the cytoplasm. Finally, it became a typical astrocyte-like type 2 OEC. We found that 16.4% of 55 astrocyte-like type 1 OECs transformed into type 2 OECs in 1 h (Figure 7E). Astrocyte-like type 2 OECs could also transform into type 1 OECs. As shown in Figure 7D, the lamellipodia on one side of this astrocyte-like type 2 OEC retracted and the lamellipodia on the other side enlarged. The cell then became a typical astrocyte-like type 1 OEC, before finally changing rapidly back to a type 2 OEC. We found that 12.2% of 41 observed astrocyte-like type 2 OECs transformed into type 1 OECs in 1 h (Figure 7E). However, in our system, we did not observe a direct transformation between Schwann cell-like OECs and astrocyte-like type 2 OECs, suggesting that astrocyte-like type 1 OECs may be an intermediate phenotype between Schwann cell-like OECs and astrocyte-like type 2 OECs.

Discussion

To examine the migratory properties of each OEC subpopulation, we developed a single OEC cell migration assay in this study. Based on time-lapse imaging of the migratory behavior of single isolated OECs, we found that distinct OEC subpopulations exhibit different migratory properties. In our studies, laminin was chosen as a substrate as it is spatiotemporally expressed in the developing olfactory nerve pathway and can have an effect on the phenotypic characteristics of OECs [25, 40-42]. Moreover, the different migratory properties were confirmed on other culture substrates, including Matrigel, collagen-gel and PLL. We also found that OECs were more motile on laminin or Matrigel than on PLL or collagen I. These results suggest that the distinct OEC subpopulations display different intrinsic migratory properties during their free migration on the same substrate.

In order to migrate, cells must be polarized [43, 44]. For example, motile T cells display a polarized morphology with polarized organization of cytoskeletal proteins such as α-tubulin [45]. In this study, we found that Schwann cell-like OECs were more motile than astrocyte-like OECs and astrocyte-like type 1 OECs were more motile than

astrocyte-like type 2 OECs. Interestingly, we also found that the cytoskeletal proteins (F-actin and microtubule) were polarized in Schwann cell-like OECs and astrocyte-like type 1 OECs, but not in astrocyte-like type 2 OECs. These polarized cytoskeletal proteins may determine the different motilities for the distinct OEC subpopulations. These results also support the notion that polarized cells, characterized by a leading lamella and a trailing tail, have better ability to migrate [43]. Using a single-cell migration assay, we demonstrated for the first time that LPA could attract Schwann cell-like OECs and astrocyte-like type 1 OECs, but not astrocyte-like type 2 OECs. These results further indicate that different OEC subpopulations have distinct migratory responses to stimulation by extrinsic factors.

OECs are described as cells that have different morphological phenotypes in cultures and transplants [4, 11, 25, 46]. However, the relationships between the different morphological phenotypes are not clear. Recent findings have demonstrated that OECs display plasticity in morphology that is dependent on environmental stimuli [4, 25, 27, 34, 47]. For example, cultured OECs underwent rapid and reversible change between a flat sheet-like morphology in the presence of serum and a fusiform bipolar morphology in the absence of serum [27, 34]. Consistent with these previous reports, different morphological phenotypes were described in our culture system. Interestingly, we found that these distinct OEC subpopulations with different migratory properties could transform into each other spontaneously. We found that these rapid morphological changes were intrinsic to OECs, but were not due to environmental stimuli based on the following evidence. First, based on time-lapse imaging, we observed the behavior of single isolated OECs, which were not attached to any other cells. Second, in our system, the temperature was held constant over time and the serum-free medium was covered by a layer of silicon oil to prevent evaporation and any change in pH. Thus, it was unlikely that any morphological change was induced by alterations to the culture conditions. Third, unlike the OECs, neurons and astrocytes showed fairly stable morphologies under the same culture conditions (data not shown). Thus, we could show that OECs display an intrinsic plasticity in morphology, which is independent of environmental stimuli. Meanwhile, we observed a direct transformation between Schwann cell-like OECs and astrocyte-like type 1 OECs, but not between Schwann cell-like OECs and astrocyte-like type 2 OECs, which suggests that astrocyte-like type 1 OECs may represent an intermediate phenotype between Schwann cell-like OECs and astrocyte-like type 2 OECs.

Our results strongly support the idea that OECs are a single type of cell with malleable phenotypes, which can transform into each other, rather than being discrete subpopulations. These rapid OEC transformations are probably mediated by the RhoA signaling pathway, as it has been found that OECs mainly adopt a flat morphology upon RhoA activation by endothelin-1, and a process-bearing morphology upon RhoA inactivation by dBcAMP [34]. Consistent with a previous report [34], we also found that dBcAMP could induce the switch from astrocyte-like OECs to Schwann cell-like OECs within 1 h in a dose-dependent manner (Supplementary information, Figure S2). Further studies are necessary to elucidate the OEC transformation mechanism.

The different migratory properties of OEC subpopulations *in vitro* may indicate their distinct functional properties *in vivo*. During development, Schwann cell-like OECs may represent newborn OECs migrating from the olfactory epithelium to the olfactory bulb. In the migration path to the olfactory bulb, either spontaneously or simulated by some extracellular factors, some of these OECs may transform into astrocyte-like type 2 OECs that have dramatically reduced motility and so stop in the olfactory pathway to serve as a substrate for axon growth or to ensheath olfactory axons. Transplanted OECs have been shown to migrate with regenerating axons through unfavorable environments in the CNS [11], and to mingle well with astrocytes in the adult brain [11, 31, 48]. Therefore, the ability of OECs to migrate in the CNS is thought to be crucial for neural regeneration and re-ensheathment after spinal cord injury. Further to this, studies have shown that several factors are involved in the regulation of OEC migration [33, 39, 49]. Transplanted OECs face a more complex environment during their migration, as they interact with a greater variety of cell types (such as reactive astrocytes) and with the many factors that are produced through injury. Our results indicate that these interactions may induce the morphology change in transplanted OECs, and/or affect their migration, which thereby influences the regeneration-promoting ability of OECs.

Interestingly, Schwann cell-like OECs but not astrocyte-like OECs have been thought to be a regeneration-promoting phenotype as they myelinate axons and promote neurite outgrowth more effectively [9, 11, 28, 50, 51]. This property of Schwann cell-like OECs may be in part due to their higher motility. In successful axonal regeneration, OECs always adopt a spindle-shaped morphology (Schwann cell-like OECs), forming a bridge or scaffold, which facilitates the growth of axons across the glial scar [11, 52]. Thus, it is of interest to test whether selectively choosing Schwann cell-like OECs for transplantation will improve the therapeutic properties of OECs in treating CNS injury. Further studies are necessary to elucidate the migratory properties of OEC subpopulations *in vivo*.

In summary, this set of experiments has demonstrated for the first time that distinct OEC subpopulations display different migratory properties *in vitro*. These results provided new evidence to support the notion of OECs as a single-cell type with malleable functional phenotypes.

Materials and Methods

Primary culture and purification of OECs

All procedures conducted on animals were approved by the Animal Experimentation Ethics Committee of Zhejiang University. Primary OEC cultures were prepared from olfactory bulbs of adult male Sprague-Dawley rats and purified by differential cell adhesiveness as described previously [32, 33]. In brief, the olfactory nerve layer was peeled away carefully from the rest of the olfactory bulb, dissociated using 0.25% trypsin (Sigma, St Louis, MO) and incubated at 37 °C for 15 min. Trypsinization was stopped by DMEM/F12 (1:1 vol/vol, Gibco, Grand Island, NY) containing 15% heat-inactivated fetal bovine serum (FBS, Hyclone, Logan, UT). The tissue was then centrifuged for 10 min at 500×*g*. The pellet was triturated using a flame-polished Pasteur pipette and plated on an uncoated 25 cm^2 culture flask twice, each time for 36 h at 37 °C in 5% CO_2. The non-adhesive cell suspension was collected and then seeded onto 35 or 60 mm dishes (Corning, LY) that were pre-coated with PLL (0.1 mg/ml, Sigma), and incubated with DMEM/F-12 containing 15% FBS as mitogen, 2 μM forskolin (Sigma) and 10 ng/ml bFGF (Sigma). The media were changed every 3 days. The overall purity of OECs was around 95% (Supplementary information, Figure S1).

OECs on substrate-coated coverslips

Cleaned square glass coverslips (8 mm) were immersed in 75% ethanol (v/v) and flame sterilized. Coverslips were coated with different substrates as follows: PLL (0.1 mg/ml, Sigma), laminin (10 μg/ml, Sigma), Matrigel matrix (50 μg/ml, BD Bioscience) or Collagen I (50 μg/ml, Cultrex) for 4-6 h at room temperature, and then washed three times with PBS. The purified OECs were re-plated onto the coated coverslips at a density of 1000 cells per coverslip. At 24 h after plating, the OECs were used for the experiments.

Immunocytochemistry and cytoskeleton staining

In brief, the purified OECs were re-plated onto the square coverslips (8 mm) coated with laminin (10 μg/ml, Sigma) at a density of 1 000 cells per coverslip, fixed with fresh 4% paraformaldehyde in 0.1 M PBS (pH 7.4) for 20 min after culturing for 24 h. After washing with PBS, cells were permeabilized with 0.2% Triton X-100 in 0.1 M PBS for 5 min, followed by incubation in blocking buffer (5% normal goat serum and 0.2% Triton X-100 in 0.1 M PBS, pH 7.4) for 1 h, and incubated overnight at 4 °C with polyclonal antibodies against GFAP (1:500, Sigma) or p-75 (1:500, Promega, Madison, WI); with a monoclonal anti-p-75 antibody (1:200, Chemicon, Temecula, CA) or acetylated tubulin (1:1 000, Sigma); or with S-100 (1:1 000, Sigma) diluted in the blocking buffer. Cells were washed three times with PBS and incubated for 1 h at room temperature with an appropriate fluorescence-conjugated secondary antibody (1:1 000, Molecular probe, Eugene, OR), and then visualized using confocal or fluorescence microscopy (FV1000, Olympus). No positive signal was observed in control incubations using no primary antibody. For visualization of F-actin, cells were incubated with rhodamine-conjugated phalloidin (1:60, Molecular probe) at room temperature for 1 h.

Characterization of OEC subpopulations

To define the OEC morphology, we adopted the following criteria [34]: Schwann cell-like OECs (process-bearing OECs) had very little cytoplasm and two or more fine processes that were longer than the width of the cell body (Figure 1A a), and astroctye-like OECs (flat OECs) had a large area of cytoplasm surrounding the nucleus and either fewer than two processes or processes that were shorter than the width of the cell body (Figure 1A b, c). In our studies, the latter could be further divided into two subtypes according to the location of the nucleus. Astrocyte-like type 1 OECs (Figure 1A b) were defined as those exhibiting a fan-like shape, with a nucleus lying at the edge of the cytoplasm and a large lamellipodium extending from the opposite side to the nucleus. Astrocyte-like type 2 OECs were defined as those having a round shape and a nucleus lying at the center of the cytoplasm (Figure 1A c). According to these criteria, we counted the total number of each subpopulation under bright-field microscopy, and counted the number of positive cells expressing OEC markers under fluorescence microscopy. The purity of each OEC subpopulation was analysed by determining the percentage of OEC subpopulations expressing the OEC markers (p-75, S-100, GFAP) from the total counted cells. Quantitative data were from three different cell cultures. Cells were counted in at least 20 randomly selected fields from one coverslip, and 100 cells for each subpopulation per coverslip ($n = 4$) were counted.

Single-cell migration assays

The gradients of factors were produced as described previously [35-37] with some modifications. In brief, the purified OEC cells were re-plated onto square coverslips (8 mm) coated with laminin (10 μg/ml) at a low density of about 1 000 cells per coverslip. At 24 h after plating, coverslips with cells were put into a chamber containing 1 ml serum-free Leibovitz's L-15 medium (L15, Gibco). The chamber was then covered with a thin layer of methyl-siloxane fluid to prevent evaporation. The experiments were carried out at the heated stage (37 °C) of a phase contrast microscope (CK40, Olympus Optial, Tokyo, Japan). Cells with a typical OEC morphology that were not attached to any other cells were selected. Micropipettes used in pulsatile ejection were pulled with a two-stage puller designed for making patch-clamp electrodes. A micropipette with a tip opening of about 1 μm was placed 15 μm perpendicular and 100 μm away from the center of the cell under test. A standard pressure pulse of 3 psi (1 psi = 6.89 kPa) in amplitude and 20 ms in duration was generated by a pulse generator and applied to the pipette at a frequency of 2 Hz. Under this standard condition, the concentration of factor at 100 μm from the pipette tip is about 10^{-3} fold lower than in the pipette [35]. LPA (Sigma) was used for pipette application at 500 μM. Images of the migrating OECs were recorded, in a time-lapse mode (one picture every 5 min interval over a total time of 60 min), with a CCD camera (JVC TK-1381; Victor Company, Yokohama, Japan) attached to the microscope, and were then stored in a computer for further analysis using Scion imaging software (Frederock, MD). Some pictures were made as movies (Windows Movie Marker software), which are presented in the Supplementary information (Movies 1-3).

We describe how to calculate the migration rate and what the migration rate ratio means (Supplementary information, Figure S3). In brief, we measured the distance of cell migration during a control

period and after treatment, and calculated the respective migration rates (total migration/time). We then calculated the migration ratio (migration rate after treatment/migration rate during the control period). The cumulative data graphs were made using MS Excel Software. Each point represents the result from one OEC, and the data were plotted from small to large. The control period was about 20 min, and the time after treatment was about 60 min.

Statistical analysis

All data presented represent results from at least three independent experiments. Statistical analysis was performed using Student's *t*-test, the Kolmogorov-Smirnov test, or using an ANOVA with pair-wise comparisons. Statistical significance was defined as $P < 0.05$.

Acknowledgments

We thank Drs Chenbing Guan and Kui Cui (Institute of Neuroscience, Shanghai Institute for Biological Science, China) for technical support in setting up the single-cell migration assay, and Dr Qian Hu (Institute of Neuroscience, Shanghai Institute for Biological Science, China) for microscopic imaging. This study was supported by the National Key Basic Research Program (2006CB500702), Ministry of Science and Technology of China (2007CB947100), National Natural Science Foundation of China (30530240 and 30770657), Program for Changjiang Scholars and Innovative Research Teams in Universities (IRT0528), and Shanghai Metropolitan Fund for Research and Development (07DJ14005).

References

1 Graziadei PP, Graziadei GA. Neurogenesis and neuron regeneration in the olfactory system of mammals. I. Morphological aspects of differentiation and structural organization of the olfactory sensory neurons. *J Neurocytol* 1979; **8**:1-18.
2 Doucette R. PNS-CNS transitional zone of the first cranial nerve. *J Comp Neurol* 1991; **312**:451-466.
3 Ramon-Cueto A, Valverde F. Olfactory bulb ensheathing glia: a unique cell type with axonal growth-promoting properties. *Glia* 1995; **14**:163-173.
4 Vincent AJ, West AK, Chuah MI. Morphological and functional plasticity of olfactory ensheathing cells. *J Neurocytol* 2005; **34**:65-80.
5 Raisman G, Li Y. Repair of neural pathways by olfactory ensheathing cells. *Nat Rev Neurosci* 2007; **8**:312-319.
6 Ramon-Cueto A, Nieto-Sampedro M. Regeneration into the spinal cord of transected dorsal root axons is promoted by ensheathing glia transplants. *Exp Neurol* 1994; **127**:232-244.
7 Smale KA, Doucette R, Kawaja MD. Implantation of olfactory ensheathing cells in the adult rat brain following fimbria-fornix transection. *Exp Neurol* 1996; **137**:225-233.
8 Ramon-Cueto A, Plant GW, Avila J, Bunge MB. Long-distance axonal regeneration in the transected adult rat spinal cord is promoted by olfactory ensheathing glia transplants. *J Neurosci* 1998; **18**:3803-3815.
9 Imaizumi T, Lankford KL, Waxman SG, Greer CA, Kocsis JD. Transplanted olfactory ensheathing cells remyelinate and enhance axonal conduction in the demyelinated dorsal columns of the rat spinal cord. *J Neurosci* 1998; **18**:6176-6185.
10 Kato T, Honmou O, Uede T, Hashi K, Kocsis JD. Transplantation of human olfactory ensheathing cells elicits remyelination of demyelinated rat spinal cord. *Glia* 2000; **30**:209-218.
11 Li Y, Field PM, Raisman G. Regeneration of adult rat corticospinal axons induced by transplanted olfactory ensheathing cells. *J Neurosci* 1998; **18**:10514-10524.
12 Franklin RJ, Gilson JM, Franceschini IA, Barnett SC. Schwann cell-like myelination following transplantation of an olfactory bulb-ensheathing cell line into areas of demyelination in the adult CNS. *Glia* 1996; **17**:217-224.
13 Lu J, Feron F, Mackay-Sim A, Waite PM. Olfactory ensheathing cells promote locomotor recovery after delayed transplantation into transected spinal cord. *Brain* 2002; **125**:14-21.
14 Navarro X, Valero A, Gudino G, *et al*. Ensheathing glia transplants promote dorsal root regeneration and spinal reflex restitution after multiple lumbar rhizotomy. *Ann Neurol* 1999; **45**:207-215.
15 Cao L, Liu L, Chen ZY, *et al*. Olfactory ensheathing cells genetically modified to secrete GDNF to promote spinal cord repair. *Brain* 2004; **127**:535-549.
16 Feron F, Perry C, Cochrane J, *et al*. Autologous olfactory ensheathing cell transplantation in human spinal cord injury. *Brain* 2005; **128**:2951-2960.
17 Valverde F, Santacana M, Heredia M. Formation of an olfactory glomerulus: morphological aspects of development and organization. *Neuroscience* 1992; **49**:255-275.
18 Astic L, Pellier-Monnin V, Godinot F. Spatio-temporal patterns of ensheathing cell differentiation in the rat olfactory system during development. *Neuroscience* 1998; **84**:295-307.
19 Chuah MI, West AK. Cellular and molecular biology of ensheathing cells. *Microsc Res Tech* 2002; **58**:216-227.
20 Key B, St John J. Axon navigation in the mammalian primary olfactory pathway: where to next? *Chem Senses* 2002; **27**:245-260.
21 Barnett SC, Chang L. Olfactory ensheathing cells and CNS repair: going solo or in need of a friend? *Trends Neurosci* 2004; **27**:54-60.
22 Au E, Roskams AJ. Olfactory ensheathing cells of the lamina propria *in vivo* and *in vitro*. *Glia* 2003; **41**:224-236.
23 Deng C, Gorrie C, Hayward I, *et al*. Survival and migration of human and rat olfactory ensheathing cells in intact and injured spinal cord. *J Neurosci Res* 2006; **83**:1201-1212.
24 Pearse DD, Sanchez AR, Pereira FC, *et al*. Transplantation of Schwann cells and/or olfactory ensheathing glia into the contused spinal cord: survival, migration, axon association, and functional recovery. *Glia* 2007; **55**:976-1000.
25 Pixley SK. The olfactory nerve contains two populations of glia, identified both *in vivo* and *in vitro*. *Glia* 1992; **5**:269-284.
26 Franceschini IA, Barnett SC. Low-affinity NGF-receptor and E-N-CAM expression define two types of olfactory nerve ensheathing cells that share a common lineage. *Dev Biol* 1996; **173**:327-343.
27 Alexander CL, Fitzgerald UF, Barnett SC. Identification of growth factors that promote long-term proliferation of olfactory ensheathing cells and modulate their antigenic phenotype. *Glia*

2002; **37**:349-364.
28 Kumar R, Hayat S, Felts P, Bunting S, Wigley C. Functional differences and interactions between phenotypic subpopulations of olfactory ensheathing cells in promoting CNS axonal regeneration. *Glia* 2005; **50**:12-20.
29 Devon R, Doucette R. Olfactory ensheathing cells myelinate dorsal root ganglion neurites. *Brain Res* 1992; **589**:175-179.
30 Ramon-Cueto A, Perez J, Nieto-Sampedro M. *In vitro* enfolding of olfactory neurites by p75 NGF receptor positive ensheathing cells from adult rat olfactory bulb. *Eur J Neurosci* 1993; **5**:1172-1180.
31 Richter MW, Fletcher PA, Liu J, Tetzlaff W, Roskams AJ. Lamina propria and olfactory bulb ensheathing cells exhibit differential integration and migration and promote differential axon sprouting in the lesioned spinal cord. *J Neurosci* 2005; **25**:10700-10711.
32 Nash HH, Borke RC, Anders JJ. New method of purification for establishing primary cultures of ensheathing cells from the adult olfactory bulb. *Glia* 2001; **34**:81-87.
33 Cao L, Su Z, Zhou Q, *et al*. Glial cell line-derived neurotrophic factor promotes olfactory ensheathing cells migration. *Glia* 2006; **54**:536-544.
34 Vincent AJ, West AK, Chuah MI. Morphological plasticity of olfactory ensheathing cells is regulated by cAMP and endothelin-1. *Glia* 2003; **41**:393-403.
35 Lohof AM, Quillan M, Dan Y, Poo MM. Asymmetric modulation of cytosolic cAMP activity induces growth cone turning. *J Neurosci* 1992; **12**:1253-1261.
36 Xu HT, Yuan XB, Guan CB, *et al*. Calcium signaling in chemorepellant Slit2-dependent regulation of neuronal migration. *Proc Natl Acad Sci USA* 2004; **101**:4296-4301.
37 Guan CB, Xu HT, Jin M, Yuan XB, Poo MM. Long-range ca(2+) signaling from growth cone to soma mediates reversal of neuronal migration induced by slit-2. *Cell* 2007; **129**:385-395.
38 Westermann S, Weber K. Post-translational modifications regulate microtubule function. *Nat Rev Mol Cell Biol* 2003; **4**:938-947.
39 Yan H, Lu D, Rivkees SA. Lysophosphatidic acid regulates the proliferation and migration of olfactory ensheathing cells *in vitro*. *Glia* 2003; **44**:26-36.
40 Julliard AK, Hartmann DJ. Spatiotemporal patterns of expression of extracellular matrix molecules in the developing and adult rat olfactory system. *Neuroscience* 1998; **84**:1135-1150.
41 Tisay KT, Key B. The extracellular matrix modulates olfactory neurite outgrowth on ensheathing cells. *J Neurosci* 1999; **19**:9890-9899.
42 Doucette R. Immunohistochemical localization of laminin, fibronectin and collagen type IV in the nerve fiber layer of the olfactory bulb. *Int J Dev Neurosci* 1996; **14**:945-959.
43 Stossel TP. On the crawling of animal cells. *Science* 1993; **260**:1086-1094.
44 Ridley AJ, Schwartz MA, Burridge K, *et al*. Cell migration: integrating signals from front to back. *Science* 2003; **302**:1704-1709.
45 Serrador JM, Nieto M, Sanchez-Madrid F. Cytoskeletal rearrangement during migration and activation of T lymphocytes. *Trends Cell Biol* 1999; **9**:228-233.
46 Raisman G. Olfactory ensheathing cells - another miracle cure for spinal cord injury? *Nat Rev Neurosci* 2001; **2**:369-375.
47 van den Pol AN, Santarelli JG. Olfactory ensheathing cells: time lapse imaging of cellular interactions, axonal support, rapid morphologic shifts, and mitosis. *J Comp Neurol* 2003; **458**:175-194.
48 Lakatos A, Franklin RJ, Barnett SC. Olfactory ensheathing cells and Schwann cells differ in their *in vitro* interactions with astrocytes. *Glia* 2000; **32**:214-225.
49 Su Z, Cao L, Zhu Y, *et al*. Nogo enhances the adhesion of olfactory ensheathing cells and inhibits their migration. *J Cell Sci* 2007; **120**:1877-1887.
50 Sasaki M, Lankford KL, Zemedkun M, Kocsis JD. Identified olfactory ensheathing cells transplanted into the transected dorsal funiculus bridge the lesion and form myelin. *J Neurosci* 2004; **24**:8485-8493.
51 Sonigra RJ, Brighton PC, Jacoby J, Hall S, Wigley CB. Adult rat olfactory nerve ensheathing cells are effective promoters of adult central nervous system neurite outgrowth in coculture. *Glia* 1999; **25**:256-269.
52 Perez-Bouza A, Wigley CB, Nacimiento W, Noth J, Brook GA. Spontaneous orientation of transplanted olfactory glia influences axonal regeneration. *Neuroreport* 1998; **9**:2971-2975.

(**Supplementary Information** is linked to the online version of the paper on the Cell Research website.)